Analysis of the jet propagation of hydrogen and helium with PFI- and DI-injectors using BOS

J. Reimer*, M Bucherer, J. Pfeil, T. Koch, Karlsruher Institut für Technologie, Institut für Kolbenmaschinen (IFKM)

Abstract

In contrast to liquid fuels, colourless gases cannot simply be made visible with a camera. For this purpose, the "Background Oriented Schlieren" method is applied. The jet images can be used to validate CFD models of gas injection, test injector components and analyse mixture formation regarding jet angle, jet shape and penetration velocity. In practice, helium is often used instead of hydrogen for jet propagation experiments, because helium is not flammable, fewer safety precautions have to be taken during the experiments and the substances have a similar density. The question now arises as to whether helium actually produces a jet image comparable to hydrogen when using a "Background Oriented Schlieren" setup. For this purpose, this paper analyses the jet propagation of both substances with a port fuel injection injector and a direct injection injector with regard to the penetration velocity and the jet surface. The direct injection injector is used with a jet cap and free nozzle. The injectors are installed in a pressure chamber in order to be able to generate counter pressures similar to a port fuel- or low pressure direct injection application. In general, it can be stated for the injectors examined that the jet dispersion is very similar for both substances and no major differences can be measured. For the port fuel injection injector as well as the outward opening nozzle of the direct injector with jet cap, the deviations between hydrogen and helium are small. In individual cases using the direct injection injector with free nozzle there are visible differences between helium and hydrogen for high chamber and injection pressures.

Kurzfassung

Im Gegensatz zu flüssigen Kraftstoffen können farblose Gase nicht einfach mit einer Kamera sichtbar gemacht werden. Zu diesem Zweck wird das „Background Oriented Schlieren“-Verfahren angewendet. Die Strahlbilder können für die Validierung von CFD Modellen der Gaseinblasung, den Test von Injektorkomponenten sowie die Analyse von Gemischbildung im Bezug auf Strahlwinkel, Strahlform und Eindringgeschwindigkeit genutzt werden. In der Praxis wird oft Helium anstelle von Wasserstoff für Strahlausbreitungsversuche benutzt, da Helium nicht brennbar ist, weniger Sicherheitsvorkehrungen bei der Versuchsdurchführung getroffen werden müssen und die Stoffe eine ähnliche Dichte besitzen. Es stellt sich die Frage, ob Helium bei der Nutzung von „Background Oriented Schlieren“ tatsächlich ein zu Wasserstoff vergleichbares Strahlbild erzeugt. Dazu wird in dieser Arbeit die Strahlausbreitung beider Stoffe mit einem Saugrohr- und Direkteinblasinjektor im Hinblick auf die Eindringgeschwindigkeit und die Strahlfläche analysiert. Der Direkteinblasinjektor wird mit Strahlkappe und freier Düse verwendet. Die Injektoren sind in einer Druckkammer verbaut, um Gegendrücke ähnlich einer Anwendung im Bereich der Saugrohr- oder Niederdruckdirekteinblasung darzustellen. Allgemein lässt sich für die untersuchten Injektoren sagen, dass die Strahlausbreitung für beide Stoffe sehr ähnlich ist und keine großen Unterschiede gemessen werden können. Beim Saugrohrventil sowie dem nach außen öffnenden Direkteinblasinjektor mit Strahlkappe sind die Abweichungen zwischen Wasserstoff und Helium gering. In Einzelfällen gibt es bei Nutzung des Direkteinblasinjektors mit freier Düse sichtbare Unterschiede zwischen Helium und Wasserstoff bei hohen Kammer- und Einblasedrücken.

1 Introduction

One of the greatest challenges today is to reduce CO_2 emissions. The heavy-duty vehicle sector in particular can contribute to this, as it accounts for a total of 27% of CO_2 emissions in the transport sector. In comparison, hydrogen internal combustion engines (HICE) have an advantage here, since battery electric vehicles (BEV) can no longer compensate for the higher CO_2 emissions produced during their life cycle. Compared to polymer electrolyte fuel cells, the costs of the hydrogen combustion engine are also lower [1, 2].

The mixture formation, specifically using low pressure direct injection (LP DI), is one of the challenges of HICEs. The hydrogen injectors are still under development and the imaging of the resulting gas jets is an important tool for this process. One method of investigating hydrogen injectors with regard to their injection characteristics is to replace the hydrogen with helium. The advantage is that helium, unlike hydrogen, is an inert and non-flammable noble gas and experiments can be carried out more easily in terms of safety issues [2]. Since the density of helium is twice as high as that of hydrogen [3, 4], it is suggested that there are differences in the resulting gas jets as well [2, 5].

The Background Oriented Schlieren (BOS) method introduced by Dalziel [6] (1998) and Meier [7] (1999) is used for analysis. Here, a random dot pattern is placed in the background of the test volume. A camera then generates a reference image in addition to the result image before the actual measurement. The two images can then be evaluated by an image correlation procedure. The displacement of the dots resulting from the deflection of the individual beams thus contains information about the spatial change in the refractive index [8]. This paper will answer the question of whether helium is a suitable surrogate for hydrogen, using BOS imaging setups, due to its similar physical properties.

2 Physical properties of hydrogen and helium

		Hydrogen	**Helium**
Molar mass	kg / mol	2.0159	4.0026
Specific gas constant	J / kgK	4124.4	2077.23
Lower heating value (grav.)	MJ / kg	119.83	-
High heating value	MJ / kg	142.19	-
Density 0 °C / 1013 mbar	kg / m^3	0.089882	0.1761
Lower heat value (vol.)	MJ / dm^3	0.010771	-
Specific heat capacity cp	kJ / kgK	14.198	5.195
Specific heat capacity cv	kJ / kgK	10.071	3.117
Heat capacity ratio		1.4098	1.666
Thermal conductivity	W / mK	0.184	0.1426
Dynamic viscosity	Ns / m^2 = kg / ms	0.00000891	1.8647E-05
Speed of sound 0°C & m/s	m / s	1261.1	967.31
Ignition temperature	°C	585	-

Table 1: Substance data for hydrogen and helium [3, 4, 9–11]

Helium is often used as a surrogate for hydrogen due to the safer handling and the reduced security measures for experimental purposes. It can be operated at the same operating pressures and is suitable as a surrogate for mixture visualization purposes. Since the physical properties of helium and hydrogen are not identical, it is suggested, that there are differences in the resulting gas jets as well. The penetration model introduced by Yip et al. suggests a reduced jet penetration velocity of -6,6 % for helium with a pressure ratio (injection pressure p and ambient pressure p_0) of $p / p_0 = 30$ [2, 5].

3 Experimental setup

In order to be able to compare the jet propagation of different injectors with different gases under engine-like pressure conditions, an optically accessible pressure chamber is used. This can be used to carry out tests at an absolute pressure of up to 4 bar. It has three access points, two of which are on one axis and equipped with sight glasses. The chamber is not heated and the experiments are carried out at room temperature.

For a better overview, the setup is shown in Figure 1. The injection beam is recorded with a high-speed camera (Phantom v1612) on which a 135 mm lens is mounted. The aperture is selected in such a way that both the background pattern and the injection beam are as sharp as possible. The background pattern is fixed to the viewing glass from the outside, which is located on the back as seen from the camera. This offers the advantage that the pattern cannot shift due to the injection. Another advantage is the possibility to change the pattern without opening the chamber.

The pattern is printed on a transparent plastic foil, which is covered with frosted glass foil from the back. This generates a more homogeneous brightness distribution and thus a better contrast between the dots and the background on the pattern. An air-cooled LED with 80 W power is used for illumination.

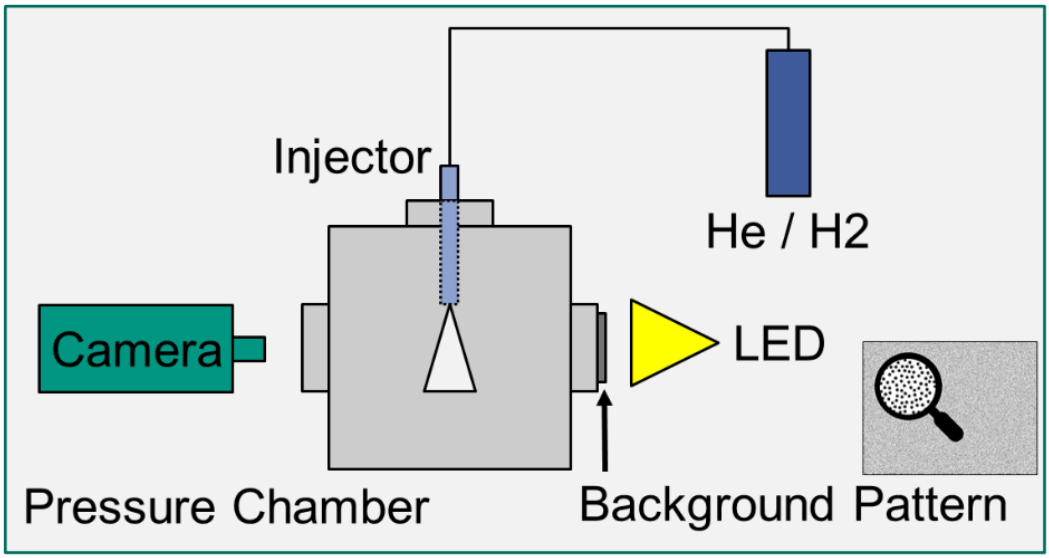

Figure 1: Set-up for BOS measurements in the pressure chamber

The injector is inserted into the chamber from the top using an adapter that is screwed to the lid of the pressure chamber. The adapter makes it possible to mount different injectors with the injector tip always in the same place. A Bosch NGI2 natural gas port fuel injection valve (PFI) and a low-pressure hydrogen direct injector (DI) are used for the tests.

The DI injector was tested in two different configurations. First with free nozzle and afterwards with a jet forming cap that has a centered single hole with a diameter of 6.4 mm. The aim is to find out whether the jet cap in front of the actual nozzle of the injector has a significant influence on the reproducibility and comparability time between helium and hydrogen. The schematic geometries of the different nozzles are shown in Figure 2.

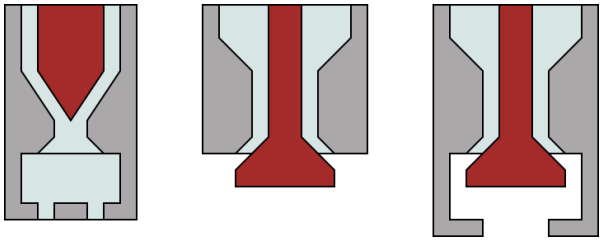

Figure 2: PFI nozzle with aperture, free nozzle and nozzle with jet forming caps

4 Experimentation

In order not to create a permanent mixture of nitrogen and the injected gas in the imaging area, the chamber is permanently flushed with a low purging flow. The synchronisation of the camera and the injector is done via a manual trigger that allows the two systems to start at the same time. The parameters from Table 2 were used for the test series. The chamber pressure is limited to 4 bar by the load limit of the pressure chamber but still represents a relevant injection point in relation to the hydrogen engine [4].

After the measurement, the images are analysed using a commercial BOS software package (based on DaVis 10 from LaVision company). The exported results are then binarised and the distance between the injector tip and the gas particle that has penetrated furthest is determined for each image. This results in the penetration depth of the injected gas over time. Since the window of the pressure chamber limits the view of the injected jet, only the first 45 mm can be observed. This is also shown by the results in chapter 5. In reality, of course, the jet penetrates further into the volume.

Through binarisation, the area of the introduced gas can also be calculated. This results from the number of pixels within the border line multiplied by the pixel size. This was determined by spatial calibration of the camera (pixel) images by means of a pattern of points with defined diameters and distances. The processing steps are shown in Figure 3.

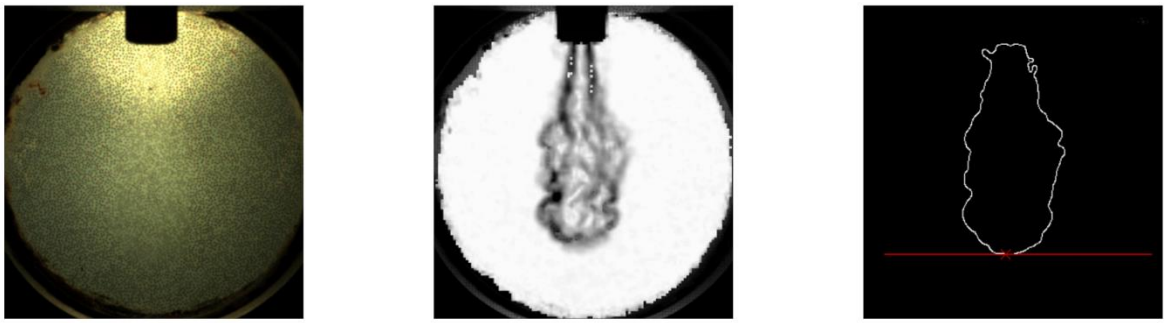

Figure 3: Overview of the postprocessing steps – Raw image, BOS image, binarized jet borders

	PFI	DI
Chamber Pressure [bar]	1; 2; 3; 4	
Gas Pressure [bar]	5; 10; 12	12; 15; 20; 25
Jet Cap [-]	-	With / Without

Table 2: Injection parameters

5 Measurements

In this chapter, 5 measuring points with the same parameters are averaged and their penetration depth or spray area is plotted over time.

5.1 PFI-Injector

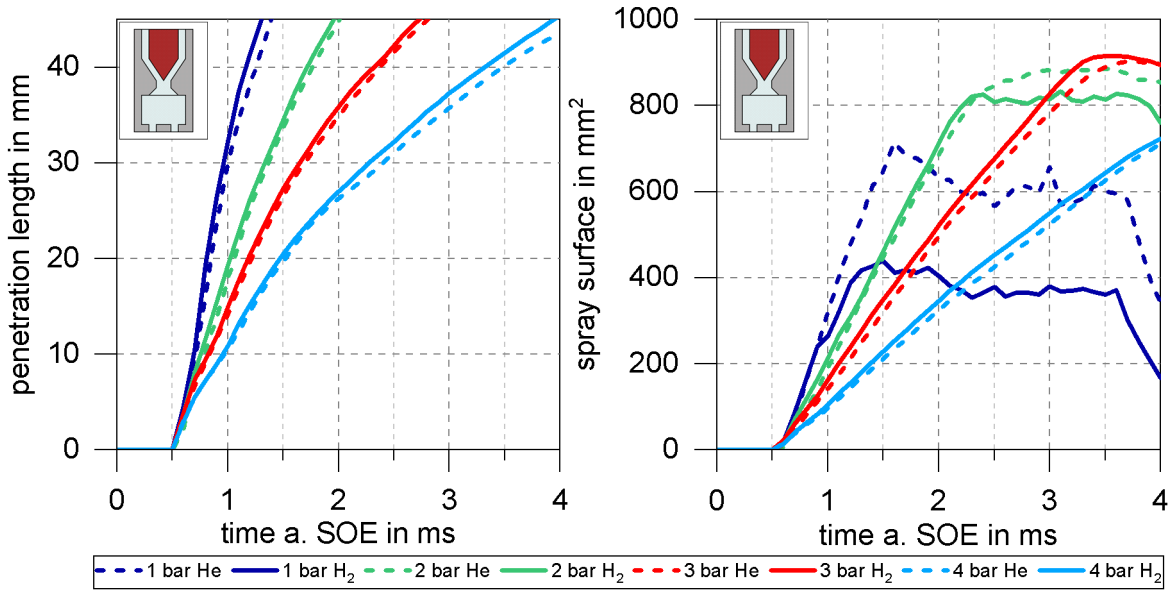

Figure 4: Penetration depth and spray area for hydrogen and helium using PFI at 5 bar injection pressure and different chamber pressures

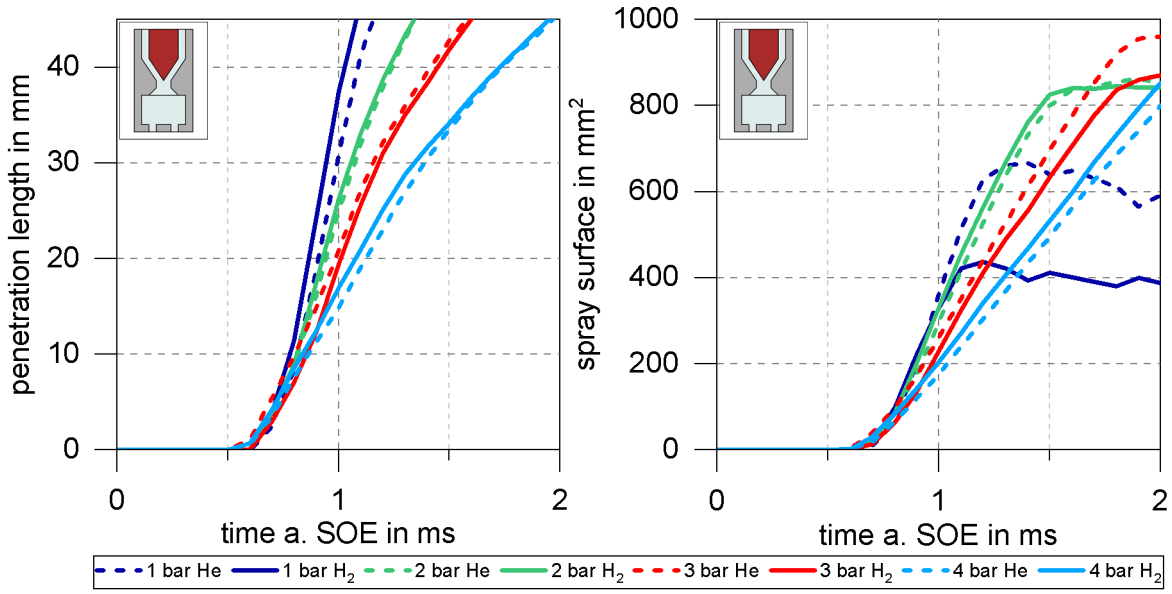

Figure 5: Penetration depth and spray area for hydrogen and helium using PFI at 12 bar injection pressure and different chamber pressures

The effect of the different chamber pressures is visible in Figure 4 (left). The injection with 5 bar shows slight deviation between hydrogen and helium. The penetration of the hydrogen jet is slightly faster than the helium jet but the deviations are still minor. Figure 5 (left) shows the jet penetrations for an injection pressure of 12 bar and different chamber pressures. The

deviations of hydrogen and helium are minor for chamber pressures of 2, 3 and 4 bar. For 1 bar chamber pressure the hydrogen jet shows a faster jet penetration than the helium jet.

For all injector and chamber pressures, injection starts at the same time. When the chamber pressure is increased, the penetration behaviour hardly changes for the first 5 to 10 millimetres. Only in the later propagation there is a noticeable difference. When opening, the first impulse of the injected gas seems to predominate. The pressure difference only becomes visible during the follow-up flow, in that the spray penetrates the chamber more slowly at higher chamber pressure.

If we look at the spray area, we see in Figure 4 and Figure 5 on the right-hand side that the area curves increase more slowly with increasing chamber pressure, but the maximum area increases. This is due to the fact that the higher chamber pressure produces a wider spray and thus a larger spray angle at the same injection pressure. The differences at 1 bar chamber pressure arise from the fact that the software has challenges detecting small density changes in certain areas at the low pressures. Since this inaccuracy occurs more strongly with hydrogen, the spray area is larger for helium. At higher chamber pressures, this measurement problem no longer occurs.

5.2 DI-Injector

When releasing a fluid from convergent and convergent-divergent nozzles such as holes at a pressure above ambient pressure, an underexpanded jet may occur. If the exit pressure of the nozzle is greater than the ambient pressure, the pressures will equalize outside the nozzle and generate an underexpanded jet. At this point the flow is in sonic state [12]. A highly underexpanded jet as shown in Figure 6 typically develops for total pressure ratio above $p / p_0 \geq 4 – 5$. A Mach disk appears just outside the nozzle that can assume different shapes, depending on the pressure ratio [12].

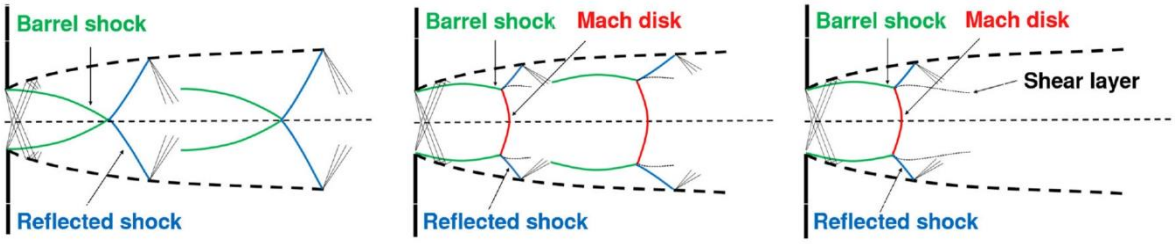

Figure 6: Different forms of underexpanded jets [13]

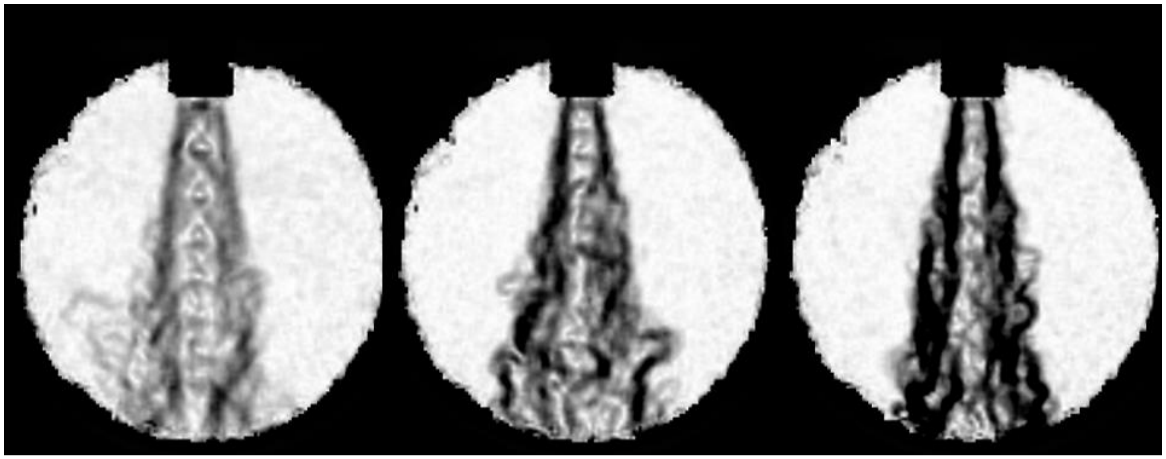

3 bar chamber pressure 20 bar injection pressure $p / p_0 = 6,7$	3 bar chamber pressure 15 bar injection pressure $p / p_0 = 5$	4 bar chamber pressure 15 bar injection pressure $p / p_0 = 3,8$

Figure 7: Jet images with hydrogen for different pressure ratios

The structure of underexpanded jets as shown in Figure 6 is also visible in the generated BOS images in Figure 7. The measurements support the statement given in Franquet et al. [12] since the described effects of underexpanded jets become visible when the pressure ratio exceeds the above mentioned threshold of $p / p_0 \geq 4 – 5$.

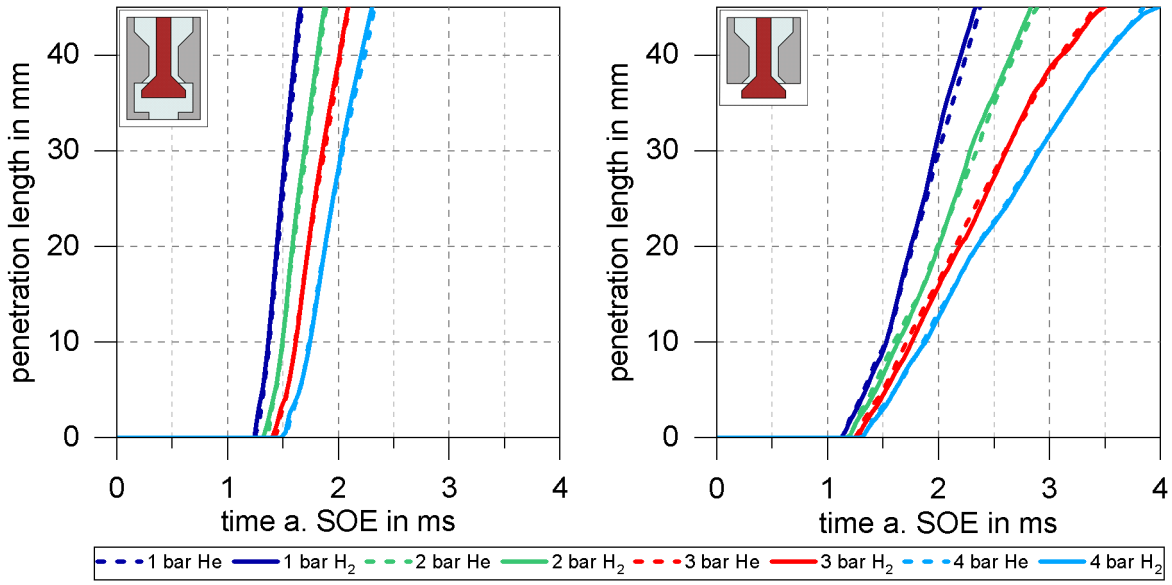

Figure 8: Penetration depth of hydrogen and helium using DI at 12 bar injection pressure and different chamber pressures

The penetration depths of the DI injector's spray (Figure 8) clearly show the influence of the chamber pressure on the start of injection. While the PFI injector with an inward opening needle is largely independent of the chamber pressure, the DI injector opens outwards into the pressure chamber. The DI injector requires more force at higher chamber pressures. As a result, the DI injector opens later at higher chamber pressures, whereby the influence with free nozzle is smaller than with jet cap. The jet cap creates a small volume between the injector nozzle and the cap opening. As a result, the gas exits the cap somewhat later than when the injector is operated with free nozzle. The exit velocity is higher because the cap concentrates the jet and reduces the exit cross-section. The differences between hydrogen and helium are minimal in both variants.

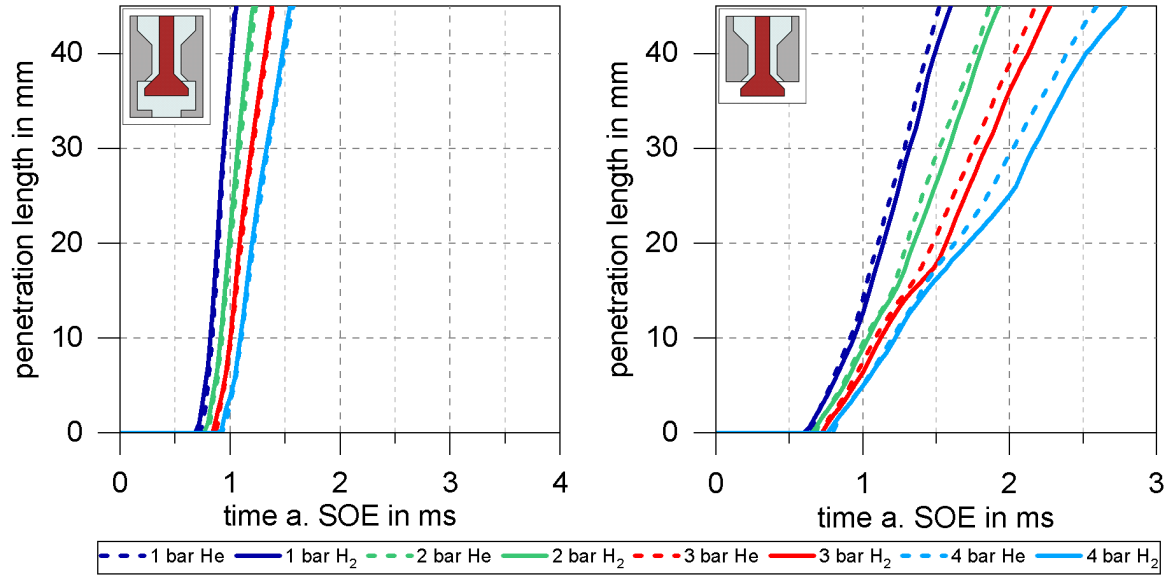

Figure 9: Penetration depth of hydrogen and helium using DI at 25 bar injection pressure and different chamber pressures

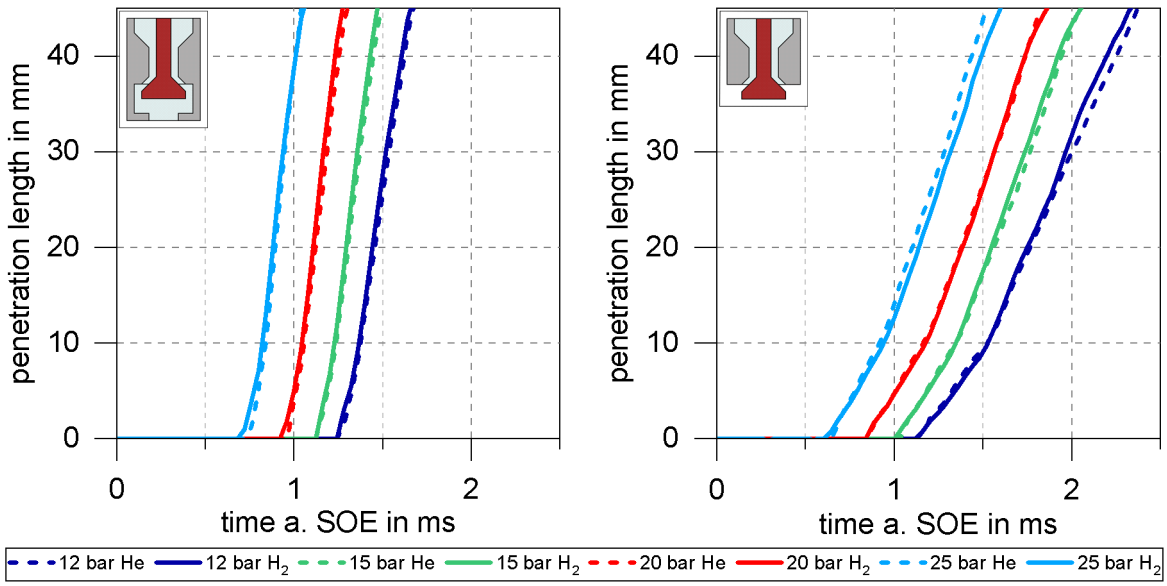

Figure 10: Penetration depth of hydrogen and helium using DI at 1 bar chamber pressure and different injection pressures

If the injector pressure is increased to 25 bar, there is still only a slight difference for the penetration depths between hydrogen and helium with the jet cap (Figure 9 left). With free nozzle (Figure 9 right) helium and hydrogen show increased deviation in penetration speed. The higher the chamber pressure, the greater the deviation between the two injected gases. Helium shows a higher penetration velocity at all pressures, albeit slightly.

Regarding the penetration depths at a constant chamber pressure of 1 bar and varying injection pressures from 12 to 25 bar, there is no appreciable difference between the injected substances. This applies for either operation with a jet cap or with free nozzle.

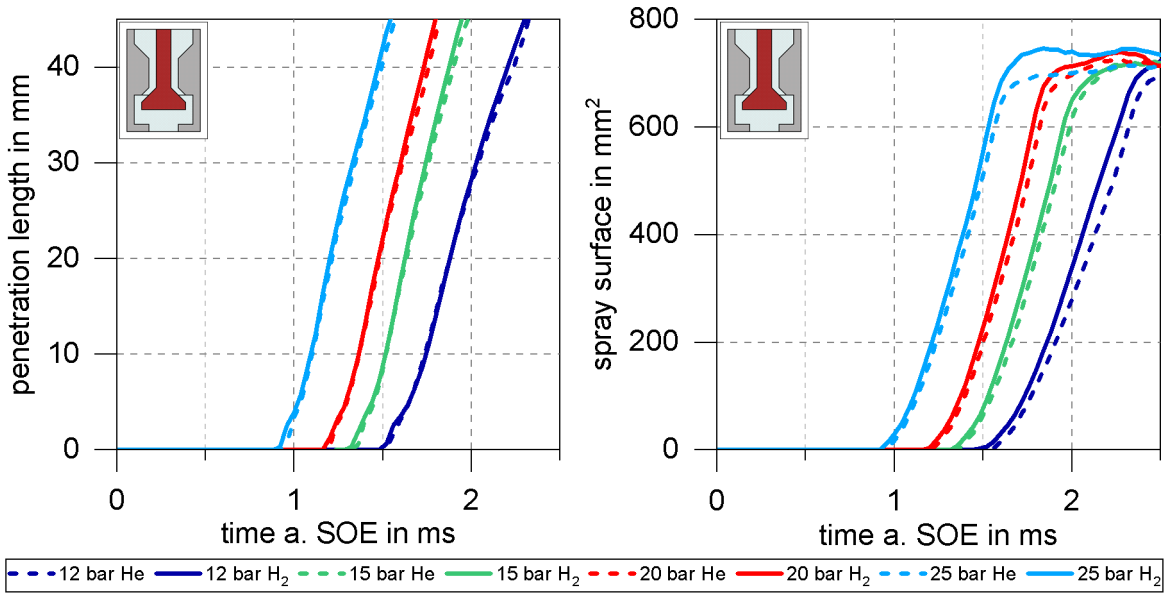

Figure 11: Penetration depth and spray area for hydrogen and helium using DI with jet cap at 4 bar chamber pressure and various injection pressures

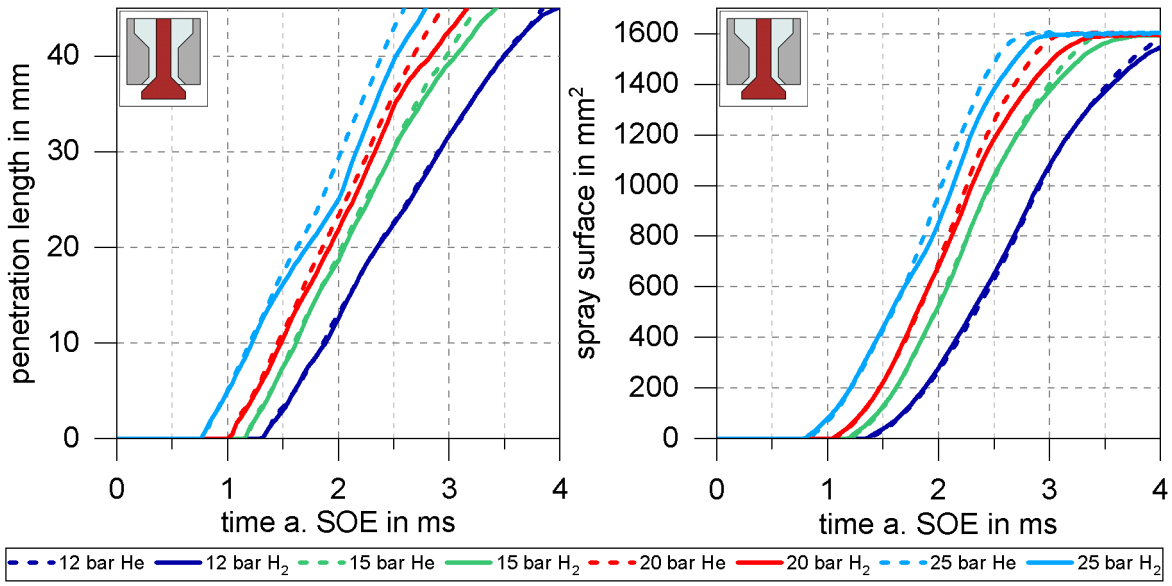

Figure 12: Penetration depth and spray area for hydrogen and helium using DI with free nozzle at 4 bar chamber pressure and various injection pressures

Figure 11 and Figure 12 show different injection pressures for 4 bar chamber pressure. The measurements show no significant deviation for the jet cap. The free nozzle on the other hand shows an increasing deviation between hydrogen and helium for higher injection pressures. The penetration speed of helium for injection pressures above 20 bar is higher than for hydrogen. In general, the deviation between hydrogen and helium seems to increase with higher chamber pressures as well as higher injection pressures.

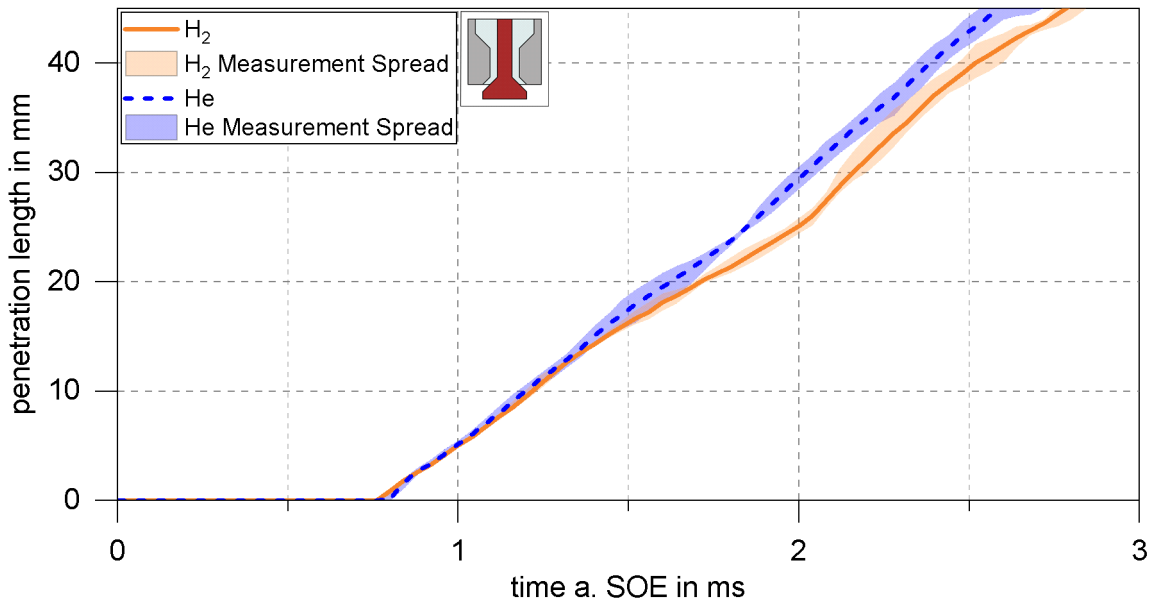

Figure 13: Measurement spread of hydrogen and helium using DI with free nozzle at 4 bar chamber pressure and 25 bar injection pressure

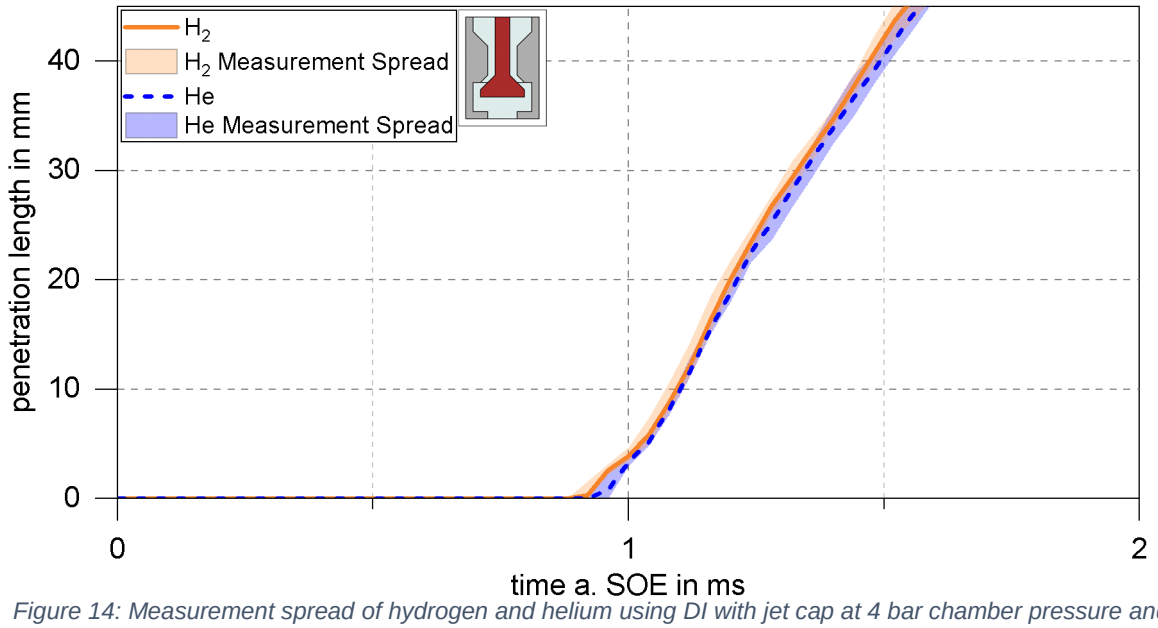

Figure 14: Measurement spread of hydrogen and helium using DI with jet cap at 4 bar chamber pressure and 25 bar injection pressure

If the penetration depths and the spray areas are analysed over time, the same relationship can be seen as with the PFI injector. Without the jet cap, the spray penetrates the pressure chamber more slowly, but due to the larger spray angle, it produces a larger spray surface with the same penetration depth.

When comparing all penetration depths and spray areas, a difference between helium and hydrogen can be seen at some operating points. It should be noted that the results show mean values, which sometimes differ in their individual penetrations, which is shown in Figure 13 and Figure 14. The minimum, maximum and mean values are shown here respectively. It can be seen in Figure 13 that the deviation is not due to high spread between the averaged measurements since the maximum measured penetration of hydrogen is still below the minimum measured penetration of helium.

Due to the small volume in the jet cap, small fluctuations in the outflow of the gas can be smoothed out and the spray flows out of the cap more evenly compared to operation with free nozzle. This is also reflected in the scatter of the penetration depths (Figure 13 and Figure 14). While the minimum and maximum values of helium and hydrogen do not cross in the injection with free nozzle, all points are close to each other in the results with cap, which speaks for the comparability of injections with helium and hydrogen.

It can be noted, that the slightly higher penetration speed of hydrogen as deduced from the model mentioned by Yip et al. can only be observed in experiments using a jet cap. For experiments using the free A nozzle, this could not be confirmed. The outlet geometry seems to be a relevant factor for the comparability of hydrogen and helium.

6 Summary & outlook

It is shown, that the BOS method applied on a pressure chamber offers the possibility to characterise jet patterns of gas fuels, like hydrogen, under real pressure conditions. The results only refer to two injectors with three different geometries. Therefore, no general statement can yet be made about the comparability of the gases using other injectors.

With the PFI injector, the differences between helium and hydrogen in injection behaviour are very small with regard to the spray surface and the penetration depth over time. The DI injector must be divided into the modes with jet cap and free nozzle. With the cap, the differences between the substances are very small, as with the PFI injector. With the free nozzle, there are operating points where the deviations become clearly visible. Looking at the spread of the single measurements, it can be stated, that the shown differences between helium and hydrogen were not due to the statistical deviation in the measurements. In these individual cases, mainly with free nozzle, there are differences between the injection with helium and hydrogen when examined closely. It can be concluded, that the outlet geometry seems to be a relevant factor for the quality of measurement with helium as a surrogate for hydrogen.

For future experiments this setup could also be used to visualize mixing processes and mixture formation inside the cylinder of a transparent engine. The results would generate a better understanding of hydrogen mixture and its effects on combustion as well as additional possibilities to validate simulation models.

7 References

[1] K. Klepatz, S. Konradt, R. Tempelhagen, and H. Rottengruber, “Systemvergleich CO2-freier Nutzfahrzeugantriebe,” in *Proceedings, Commercial Vehicle Technology 2020/2021*, K. Berns, K. Dressler, R. Kalmar, N. Stephan, R. Teutsch, and M. Thul, Eds., Wiesbaden: Springer Fachmedien Wiesbaden, 2021, pp. 171–191.

[2] M. Brauer *et al.,* “Optimization of the mixture formation in DI hydrogen combustion engines by modified injector nozzle design,” in *31st Aachen Colloquium Sustainable Mobility 2022*, Oct. 2022.

[3] R. Harth and K. Hammeke, “Thermodynamische Stoffwerte von HELIUM im Bereich von 0 bis 3000° C und 0,2 bis 200 bar,” Jülich, Berichte der Kernforschungsanlage Jülich Juel-0666-RB, 1970.

[4] H. Eichlseder and M. Klell, *Wasserstoff in der Fahrzeugtechnik: Erzeugung, Speicherung, Anwendung*: Vieweg+Teubner Verlag, 2008.

[5] H. L. Yip *et al.,* “A Review of Hydrogen Direct Injection for Internal Combustion Engines: Towards Carbon-Free Combustion,” *Applied Sciences*, vol. 9, no. 22, p. 4842, 2019, doi: 10.3390/app9224842.

[6] S. B. Dalziel, G. O. Hughes, and B. R. Sutherland, “Synthetic Schlieren [Konferenzbeitrag],” in *Proceedings of the 8th international symposium on flow visualization*, 1998, 62.1-62.6.

[7] G. E. A. Meier, “Schlieren measuring process detects changes in turbulent atmospheric flow, aerodynamic, chemical processing and environmental pollution,” DE19942856 (A1), DE DE19991042856 19990908, Jun 21, 2000.

[8] M. Raffel, “Background-oriented schlieren (BOS) techniques,” *Experiments in Fluids*, vol. 56, no. 3, pp. 1–17, 2015, doi: 10.1007/s00348-015-1927-5.

[9] J. W. Leachman, R. T Jacobsen, E. W. Lemmon, and S. G. Penoncello, “Helium,” in *International Cryogenics Monograph Series, Thermodynamic Properties of Cryogenic*

Fluids, J. W. Leachman, R. T. Jacobsen, E. W. Lemmon, and S. G. Penoncello, Eds., 2nd ed., Cham: Springer International Publishing, 2017, pp. 23–39.
[10] T. Schmidt, *Wasserstofftechnik*: Carl Hanser Verlag GmbH & Co. KG, 2022.
[11] A. Banerjea, A. Stoehr, N. Hüpping, K. Hammeke, and H. E. Kipke, “Thermodynamische Stoffwerte von Helium im Bereich von 20 bis 1500 Grad C und 1 bis 100 bar,” 1978.
[12] E. Franquet, V. Perrier, S. Gibout, and P. Bruel, “Free underexpanded jets in a quiescent medium: A review,” *Progress in Aerospace Sciences*, vol. 77, pp. 25–53, 2015, doi: 10.1016/j.paerosci.2015.06.006.
[13] G. Anaclerio, T. Capurso, M. Torresi, and S. M. Camporeale, “Numerical characterization of hydrogen under-expanded jets with a focus on Internal Combustion Engines applications,” *International Journal of Engine Research*, 2023, doi: 10.1177/14680874221148789.